Orbital-selective electronic localization in dimerized NbO_2: From Peierls to Mott

L. Craco
Institute of Physics, Federal University of Mato Grosso, 78060-900, Cuiabá, Mato Grosso, Brazil

(Received 22 January 2024; revised 6 June 2024; accepted 7 June 2024; published 20 June 2024)

We present a theoretical investigation of the t_{2g} electronic structure reconstruction of body-centered-tetragonal (bct) NbO_2 employing a combination of density functional theory and dimer-embedded dynamical mean-field theory calculations. We describe the electronic structure of the insulating phase of bct NbO_2 and propose an orbital-selective mechanism for the gap opening. The resulting insulating state of the dimerized x^2-y^2 orbital along the rutile c axis is shown to be adiabatically connected to an entangled Mott-Peierls insulator, but the true nature of insulating bct NbO_2 compared with experiment is better characterized as a Mott localized electronic state due to strong dynamical intrasite multiorbital correlations. Our orbital-selective, strong-coupling scenario could be tested in future studies of NbO_2 Mott memristors for neuromorphic computing.

DOI: 10.1103/PhysRevB.109.235136

I. INTRODUCTION

A problem of fundamental importance in the field of Mott materials and associated insulator-to-metal [1] process(es) is to understand why itinerant electrons, which interact with one another via Coulomb interactions, suddenly transform the mobile electronic state into an insulator in which the electrons are bound to individual atomic or lattice sites. Historically, lot of effort has been made to precisely characterize this transition [2]. Extant developments following the discovery of high-T_c cuprates have considerably enriched this issue and led to major reassessments in our view of Mott insulators. [2]

Among the increasing number of transition-metal oxides showing first-order metal-insulator instabilities [2,3], one of the most prominent examples within the transition-metal dioxide family is VO_2, which undergoes a first-order metal-insulator transition with decreasing temperature [4]. The high-T metallic phase has a tetragonal rutile-type structure, which is reduced to monoclinic at the first-order transition occurring around 340 K [2]. The crystal structure of rutile VO_2 is formed by equally spaced vanadium atoms sitting at the center of edge-sharing oxygen octahedra that form linear chains along the rutile c axis. The tetragonal crystal field splits the $3d$ manifold into two higher e_g and three lower t_{2g} levels. In the $3d^1$ electronic state, the single valence electron of vanadium can therefore occupy any of the three t_{2g} orbitals, i.e., the singlet a_{1g} and doublet e_g^π orbitals. The monoclinic phase, on the other hand, is characterized by an antiferroelectric displacement [5,6] of each vanadium away from the center of the octahedra, and the linear chains become zigzag and start to dimerize [7]. According to Ref. [8], the basal-plane component of the antiferroelectric distortion raises the energy of the e_g^π orbitals with respect to a_{1g}. Moreover, the linear chain distortion along the rutile c axis, which drives the chain dimerization, opens a gap between bonding and antibonding combinations of the a_{1g} orbital sector. Thus, for a sufficiently large crystal-field splitting the bonding combination of a_{1g} fills completely, while the antibonding combination and e_g^π become empty, giving rise to the insulating electronic state. According to this viewpoint, [8] the metal-insulator transition in VO_2 relies on a single-particle description, in which, due to the Peierls instability, the quasi-one-dimensional a_{1g} band becomes half filled while the e_g^π orbitals are nearly fully polarized via enhanced crystal-field effects. However, how robust this one-band picture is to dynamical effects arising from short-range, intersite correlations as well as to changes in orbital polarization via the interorbital proximity effect induced by U' and J_H (see our discussion below) remains an open problem. This is partially caused by the fact that Mott-Hubbard (dynamical correlations) [1,9] and Peierls (structural distortion) [8] physics are understood to play essential roles and possibly to interact in this transition since the lattice distortion appears to be aided [6,10,11] by the presence of strongly correlated electronic states in close proximity to Mottness [12–14].

Historically, the metal-insulator transition in VO_2 has long been the subject of a lively controversy, and whether it is dominantly a Mott transition [9] or one driven by lattice dimerization effects arising from structural effects [8] that promote the dimer pairing along the c axis of the rutile phase [15] remains hotly debated. It is noteworthy that a soft-x-ray absorption spectroscopy studies have found a sudden change in the t_{2g} orbital occupations across the orbital-assisted metal-insulator transition in VO_2 [16], suggesting that multiorbital (MO) degrees of freedom also play an important role within the monoclinic phase of VO_2 [6,12,17]. In this work we show that a dynamically reconstructed many-particle electronic state induced by MO electron-electron interactions [18,19] plays a central role in determining the orbital-selective nature of the distorted rutile [body-centered-tetragonal (bct)] phase of NbO_2. Specifically, based on density functional plus dynamical mean-field theory (DFT+DMFT) [20] calculations, we show how the active $4d$ orbitals of bct NbO_2 [21,22] are reshaped due to sizable electron-electron interactions. In contrast to earlier studies [18,23–26], the question we address here is how the electronic structure of bct NbO_2 [21,22] is reconstructed by the interplay between antiferroelectric displacements [27] and MO dynamical correlations [19], showing the emergent orbital-selective electronic localized phase.

NbO_2 undergoes a metal-insulator transition at temperatures between 810 and 1081 K [3,25,28], which comes along with a structural transition from the low-temperature, insulating distorted rutile ($I4_1/a$) to a metallic regular rutile ($P4_2/mnm$) structure [29]. Similar to VO_2, the structural transition in NbO_2 is accompanied by the formation of Nb-Nb pairing along the c direction due to the antiferroelectric tilt, which leads to a Peierls dimerization in the electron localized state. Thus, motivated by earlier studies [6,12,16], in a recent work we considered the insulator-metal transition of NbO_2 as a Mott-Hubbard transition triggered by large spectral changes accompanying small changes in the antiferroelectric distortion [30]. Good qualitative agreement with both the switch in orbital occupations and the one-particle spectral function seen in experiment was found. In particular, an orbital-selective electronic state was predicted to emerge without Fermi liquid quasiparticles. While this could explain the incoherent, pseudogaplike metallicity seen in rutile NbO_2 [25], it could not capture nonlocal dynamical effects associated with dimerization in the bct phase, an effect described using a combination of DFT and embedded cluster-DMFT methods in Ref. [18]. Interestingly, due to the absence of poles (as in classical Mott insulators) [11] in the frequency dependence of the self-energy's imaginary parts, it was suggested in Ref. [18] that in the insulating bct phase, once the dimerization occurs, the Mott instability is arrested and, therefore, it should be interpreted as a correlation-enhanced Peierls transition [10]. However, a more recent study [19] concluded that the insulating state of baddeleyite-type NbO_2, a distorted ZrO_2-type structure, is dominantly driven by electronic correlation effects. These combined studies have spawned an interesting question: Is Mott physics or correlation-assisted Peierls dimerization the basic driving force for the insulating state in bct NbO_2? Here, we shed light on this problem, showing the electronic structure evolution with increasing MO electron-electron correlation effects on the dimerized bct phase of NbO_2, which is relevant for future Mott memristors [31].

For the sake of clarity, we note here that NbO_2 is regarded as a promising material for applications in memory devices [32] and neural-inspired computing [33]. As discussed in Ref. [19], the neuromorphic computing principle was motivated by the discovery of Mott-based memristors that replicate the voltage triggered switching behavior observed in biological ion channels that enabled a physical neuristor circuit to be built [34]. NbO_2 memristors are known to successfully replicate the rectification observed in voltage-gated biological ion channels [35] and the hysteresis necessary for operation of the neuristor circuit [34], supporting the view that NbO_2 is a promising candidate system for future neuromorphic computing [31].

The evolution of electronic spectra and band gap formation across the metal-insulator transition in NbO_2 has been experimentally explored in recent years [25,26,36]. Reference [25] showed a metallic state with pseudogaplike features at low energies evolving into a localized state at lower temperature. In the insulator, the $4d$ valence band is narrowed and shifted downward by approximately 0.4 eV across the structural phase transition, which, according to Ref. [25], is a Peierls-driven metal-insulator transition. In this work we follow the route outlined in Ref. [18] to study the correlated electronic structure reconstruction of bct **NbO_2**. From an analysis of the results we propose a many-body picture of the strongly correlated insulating state in this system. It is based on the antiferroelectric displacement of the NbO_6 octahedra which (for a given total occupation of t_{2g} orbitals) is renormalized by MO electron-electron interactions, resulting in changes in orbital occupations and orbital polarization not outlined in Ref. [18]. We also show how good quantitative agreement with the integrated photoemission and inverse-photoemission spectra is also obtained within our dimer-embedded DFT+DMFT framework.

II. THEORY AND RESULTS

To treat Nb-Nb pairing along the c direction [18,21,22] in bct NbO_2 we consider the dimer Hubbard model [37], which is a natural extension of the single-band Hubbard model. The dimer Hubbard model is known to capture the competition between Mott localization due to intrinsic Coulomb repulsion and singlet dimerization, i.e., the Peierls localization. The key feature is that in the one-band case there is a single site in the unit cell, while in the dimerized case there is a Mott-molecular dimer [38]. This leads to a system in which two copies of the Hubbard model are coupled at every site by an intradimer hopping $t_\perp$ [39,40]. In the limit of $t_\perp \to 0$ the two copies become independent, and one recovers the physics of the conventional single-site Hubbard model [41].

The dimer Hubbard model in terms of second quantization operators is defined as [39,40,42] $\bar{H} = [-t\sum_{\langle i,j\rangle,\alpha,\sigma} c^\dagger_{i,\alpha,\sigma}c_{i,\alpha,\sigma} + t_\perp \sum_{i,1\sigma} c^\dagger_{i,1,\sigma}c_{i,2,\sigma} + \text{H.c.}] + U\sum_{i,\alpha} n_{i,\alpha,\uparrow}n_{i,\alpha,\downarrow}$, where $\langle i, j\rangle$ denotes the nearest-neighbor lattice sites, $\alpha = 1, 2$ denote the dimer orbital within a given site, σ is the spin, t is the lattice hopping, and U is the on-site Coulomb repulsion. With these caveats, the corresponding free electron ($U = 0$) retarded Green's function for the x^2-y^2 orbital of bct NbO_2 can be written as $G_\alpha(\omega, \mathbf{k}) = [\xi_\alpha(\omega) - \frac{t_\perp^2}{\xi_\beta(\omega)} - \varepsilon_{x^2-y^2}(\mathbf{k})]^{-1}$. Here, $\xi_\alpha(\omega) \equiv \omega + i0^+ + \mu - \varepsilon_\alpha$, ε_α is the on-site energy of the dimer orbital α [42], $\alpha, \beta = 1, 2$, $\varepsilon_{x^2-y^2}(\mathbf{k})$ is the rutile bare band dispersion of the x^2-y^2 orbital [21], and μ is the chemical potential. To ensure that the leading edge of the dimerized bonding band (see the results below) is located exactly below the Fermi level ($E_F = \omega = 0$) we set $\varepsilon_\alpha = \varepsilon_\beta = 0.35$ eV, implying that $\xi_\alpha(\omega) = \xi_\beta(\omega)$.

The bare Green's function above describes the noninteracting limit of the Hubbard dimer [37] composed of two bands which, like in the periodic Anderson model [41,43], are locally hybridized via $t_\perp$ at every lattice site. Thus, starting with the unperturbed rutile electronic structure [21] at finite $t_\perp$, this leads to a direct bonding-antibonding band splitting, as shown in Fig. 1. This is the Peierls-like mechanism, as it is driven by the increase in the intradimer hopping amplitude $t_\perp$, where dimers in the unit cell form a molecular bond that locks the conduction electron degree of freedom [8]. While within DFT [21,22] the bonding band is half filled, we find within our Green's function treatment a smaller band filling $n_{x^2-y^2} = 0.7$, suggesting that hidden multiband proximity effects not considered within our framework might be relevant for bct

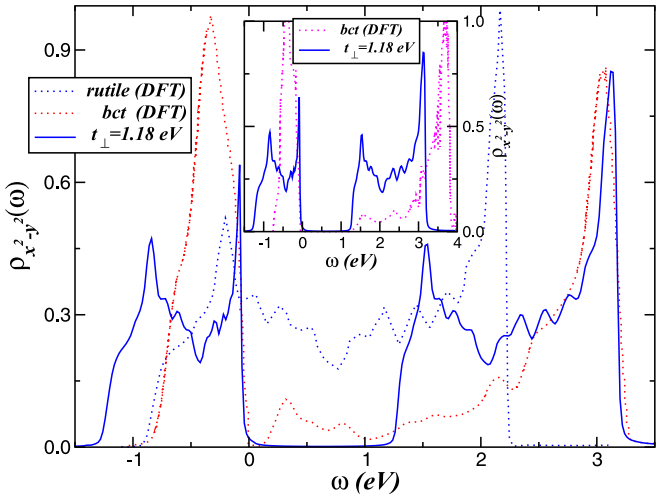

FIG. 1. Comparison of DFT spectra taken from Refs. [21] (main panel) and [22] (inset) and our result for the dimerized density of states (DOS) of the x^2-y^2 orbital of body-centered-tetragonal (bct) NbO_2. (The DFT DOS of rutile NbO_2 is shown for comparison in the main panel). Note in the inset the good agreement for the bare band gap size for the dimerized x^2-y^2 orbital of bct NbO_2.

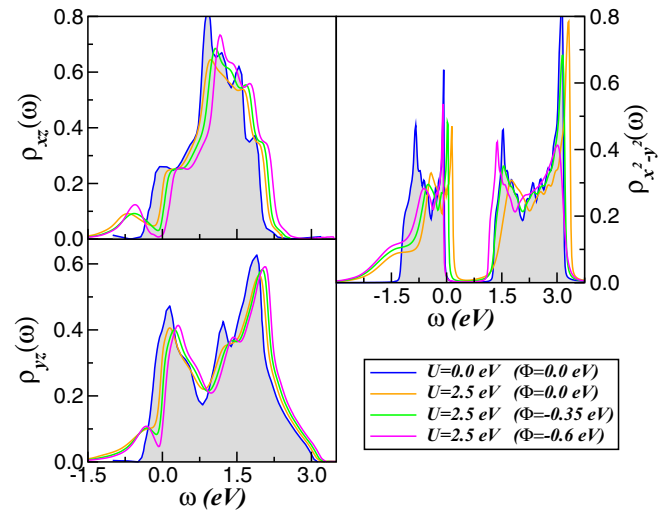

FIG. 2. Orbital-resolved DOS of bct NbO_2, showing its evolution for different values of the Coulomb interaction U and the trial antiferroelectric displacement Φ [12]. Apart from orbital selectivity, a particularly interesting feature is the emergence of lower Hubbard bands on all t_{2g} orbitals and the robustness of the dimerized one-particle band gap to small changes in U and Φ. (The unperturbed DFT bare DOS used as input for DFT+DMFT calculations is taken from Ref. [21]). Here, all DFT+DMFT(MO-IPT) spectral functions are computed at zero temperature.

NbO_2. Earlier studies on VO_2 also suggested that the metal-insulator transition results predominantly from the increased p-d overlap stemming from the antiferroelectric distortion of the VO_6 octahedra [5]. In Fig. 1 it is also worth noting the width of the bonding band, which is slightly larger than for the DFT results. However, as seen in the inset of Fig. 1 our choice of $t_\perp$ correctly accounts for the bonding-antibonding gap size obtained in Ref. [22], providing support for our Green's function formalism for the dimerized x^2-y^2 orbital of bct NbO_2.

To explore orbital selectivity in bct NbO_2 we use orbital-resolved DFT results for the metallic crystal structure [21], with lattice constants and atomic positions obtained for a rutile-type structure [29], as input for DFT+DMFT [19]. Within our formalism the projected DOS in Fig. 2 for $U = 0$ shows that the (higher in energy) xz and yz orbitals in this $4d^1$ compound have appreciable spectral weight near E_F. In contrast to Refs. [21,22], in which the xz and yz orbitals of bct NbO_2 were found to be almost fully polarized, here, we keep them metallic to account for the correct total one-electron band filling n of the $4dt_{2g}$ shell ($n_{t_{2g}}$) of NbO_2. An interesting aspect in the bare DFT DOS we use here as input for DFT+DMFT calculations [19] is the nearly one-dimensional-like dispersion of the x^2-y^2 orbital parallel to the rutile c axis, [21] as shown in the main panel of Fig. 1. Moreover, as seen in Fig. 2, the bare dispersion of the xz orbital is characterized by a single broad structure, while the yz DOS displays a structure with two maxima, one slightly above E_F and the other at 1.9 eV. How these t_{2g} electronic channels with nearly metallic (xz, yz) and $t_\perp$-induced x^2-y^2 bonding-antibonding bands are reshaped by the interplay between antiferroelectricity and local many-particle correlations is our focus here.

Like in Refs. [19,30], local MO interactions in NbO_2 are contained in $H_{\rm int} = U\sum_{i,a} n_{i,a,\uparrow}n_{i,a,\downarrow} + U'\sum_{i,a\neq b} n_{i,a}n_{i,b} - J_H\sum_{i,a\neq b}\mathbf{S}_{i,a}\cdot\mathbf{S}_{i,b}$, where $a = (x^2\text{-}y^2, yz, xz)$ denote the diagonalized t_{2g} orbitals of rutile NbO_2 [21] and, as in $\bar{H}$ above, U is the intraorbital Coulomb repulsion, $U' = U - 2J_H$ is the interorbital Coulomb interaction term, and J_H is Hund's coupling. Given the complexity of the MO problem, with diagonal and off-diagonal lattice Green's functions and self-energies [44], here, we work in the basis that diagonalizes the one-particle density matrix. In this basis interorbital one-electron overlap is zero, so in the paramagnetic phase we have $G_{a,b,\sigma}(\omega) = \delta_{a,b}G_{a,\sigma}(\omega)$ [45]. We evaluate the many-particle Green's functions $G_a(\omega,\mathbf{k}) = [\xi_a(\omega) - \frac{t_\perp^2}{\xi_a(\omega)}\delta_{a,x^2-y^2} - \varepsilon_a(\mathbf{k})]^{-1}$ of the t_{2g} MO Hamiltonian of bct NbO_2 within DFT+DMFT [20]. Here, δ_{a,x^2-y^2} typify the dimer-embedded MO DFT+DMFT framework, and $\xi_a = \omega + i0^+ + \mu - \varepsilon_a - \Sigma_a(\omega)$ [46]. As in Refs. [19,30], the many-particle problem of bct NbO_2 is treated using the MO iterated perturbation theory (MO-IPT) as an impurity solver for DMFT [43], which accounts for local intrasite and MO (both static and dynamic) renormalizations on the bare ($U = 0$) spectral functions shown in Fig. 2. The equations for the MO-IPT self-energies $\Sigma_a(\omega)$ can be found, for example, in Ref. [43], so we do not repeat the equations here. This real-frequency perturbative ansatz has a proven record of good semiquantitative agreement with experiment for a range of correlated materials, and it gives results in qualitatively agreement with numerical exact continuous-time quantum Monte Carlo calculations for the tetragonal FeSe superconductor [47], in spite of the fact that fully charge self-consistent DFT+DMFT calculations are presently unreachable within our scheme.

Let us now discuss our DFT+DMFT results obtained within the d^1 electronic configuration of the bct NbO_2 parent

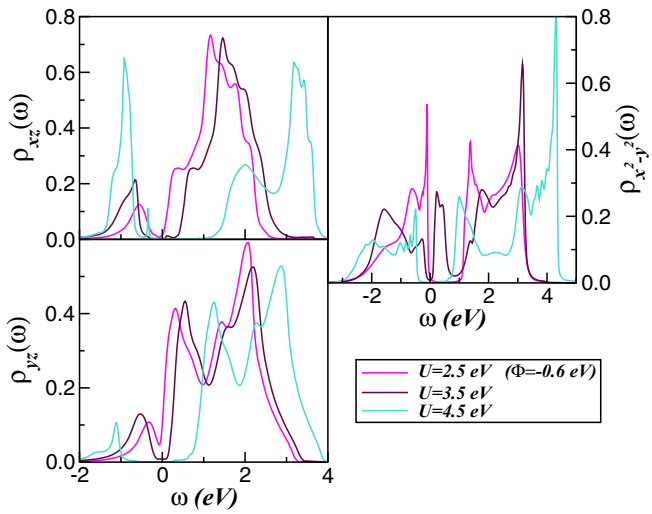

FIG. 3. Orbital-resolved DFT+DMFT DOS of bct NbO_2, showing its evolution with increasing U at fixed Φ. A particularly interesting feature is the large spectral weight transfer with increasing U. Apart from Mott (xz, yz) and assisted Mott-Peierls (x^2-y^2) electron localization, a relevant feature is the spectral weight transfer on all orbitals with increasing U and the reversal of orbital polarization between the xz and x^2-y^2 orbitals at $U = 4.5\,\text{eV}$.

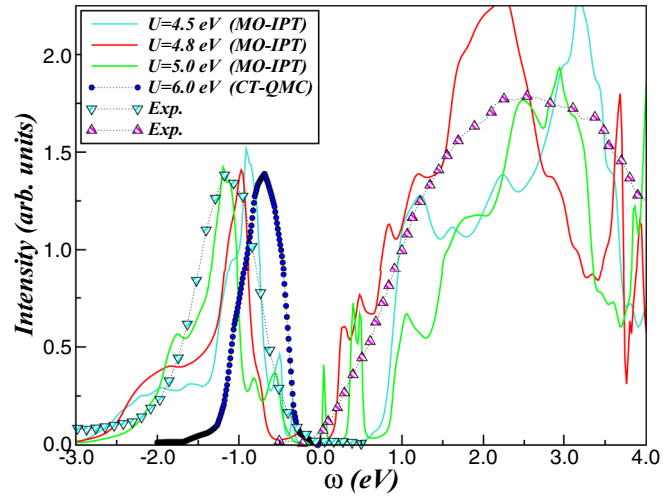

FIG. 4. Theory and experiment comparison between the DFT+DMFT results and hard x-ray photoelectron spectroscopy (HAXPES, downward triangles) and x-ray photoelectron spectroscopy (IPS, upward triangles) measurements taken from Refs. [25,52], respectively. Note the good qualitative theory-experiment agreement for the peak position of the lower Hubbard band close to -1.2 eV, as well as the upper Hubbard band main peak position at 2.5 eV for $U = 5.0\,\text{eV}$, which almost coincides with experiment. DFT+DMFT (CT-QMC) total valence band spectra [18] are also shown for comparison. [The HAXPES and DFT+DMFT (CT-QMC) curves have been normalized so that they have the same intensity.]

compound. In Fig. 2 we display the effect of electron-electron interactions on the active x^2-y^2, xz, and yz orbitals of bct NbO_2. According to our DFT+DMFT results, at $U = 2.5\,\text{eV}$ (and $J_H = 1.0\,\text{eV}$) [48] bct NbO_2 is metallic, with all t_{2g} orbitals showing spectral weight at E_F. As in Ref. [26], electron correlations were found to distribute electrons more evenly among the three t_{2g} orbitals, a characteristic akin to the interorbital proximity effect induced by U' and J_H. Thus, in order to reduce correlation-driven orbital depolarization effects [49], we consider in our self-consistent many-particle scheme the role played by antiferroelectric displacement Φ along the c axis [27], which enhances the splitting of the t_{2g} orbitals at the local level [9,12]. Thus, starting with a trial value of $\Phi \equiv \Phi_{x^2-y^2} \neq 0.0$ (and $\Phi_{xz,yz} = 0.0$), MO correlations have two important effects in this situation. Given a trial value of Φ, interorbital interactions renormalize its bare value via Hartree shifts, inducing changes in the orbital occupations and, more importantly, large changes in spectral weight transfer (driven by the dynamical nature of strong local correlations) upon small changes in Φ, as shown Fig. 2. It is clear in Fig. 2 that for $\Phi = -0.6\,\text{eV}$ the Peierls-like insulating state is restored with the concomitant downshift of the x^2-y^2 one-particle spectral function and enhanced incoherent lower Hubbard band features at energies close to 1.5 eV binding energy. An additional interesting feature that can be seen in Fig. 2 is the degree of electron correlation effects on the active t_{2g} orbitals of bct NbO_2. At $U = 2.5\,\text{eV}$, the x^2-y^2 orbital is found to be the less correlated one, due to dimerization-induced enhancement of the bare bandwidth $W_{x^2-y^2}$ effectively reducing the correlation to a bandwidth ratio in this orbital sector. The opposite trend holds true for the xz orbital, giving rise to an orbital-selective Mott localized state at $U = 2.5\,\text{eV}$.

For a more detailed analysis of dynamical MO correlation effects in bct NbO_2, in Fig. 3 we display the changes in the orbital-resolved spectral functions induced by increasing U from 2.5 to 4.5 eV with fixed $\Phi = -0.6\,\text{eV}$. As seen in Fig. 3, MO electronic correlations lead to large modifications of the correlated spectra, in particular for the xz orbital which shows enhanced spectral weight transfer below E_F that is a consequence of the intricate interplay between the correlation and structural aspects in MO systems [30,50]. As seen in the bottom left panel of Fig. 3, while the yz orbital loses its spectral weight, the DFT+DMFT solution obtained for $U = 4.5\,\text{eV}$ and $\Phi = -0.6\,\text{eV}$ is characterized by a reversal of orbital polarization between the x^2-y^2 and xz orbitals [51]. The latter shows enhanced spectral weight below E_F, which is visible in top left panel of Fig. 3. It is also worth noting the near suppression of the Peierls-like band gap in the x^2-y^2 orbital for $U = 3.5\,\text{eV}$, given the trend toward entangled Mott-Peierls localization with increasing U. Thus, as seen in Fig. 3, the correlation-induced interorbital proximity effect results in orbital-dependent redistributions of electron occupations and spectral weights, which pushes bct NbO_2 into an orbital-selective insulating state with coexisting Mott localized (xz, yz) and entangled Mott-Peierls (x^2-y^2) electronic states.

To compare our DFT+DMFT results to published experimental data [25,52], we repeat our calculation for $\Phi = -0.6\,\text{eV}$ using $4.8 \leqslant U \leqslant 5.0\,\text{eV}$ and $J_H = 1.0$ eV. The higher U is consistent with the effective strength parameter $U_{\text{eff}} \equiv U - J = 5.0\,\text{eV}$ reported in Ref. [53]. In Fig. 4 we show our results for the one-electron spectral function along with continuous-time quantum Monte Carlo (CT-QMC) [54]

and the experimental [25,52] results. First, looking at the total valence band DOS result for bct NbO_2 from Ref. [18], we find that a good fit to the main peak of the hard x-ray photoelectron spectroscopy (HAXPES) spectrum for the bct phase of NbO_2 [25] is possible only upon a downward shift of the CT-QMC curve by 0.3 eV. On the other hand, as seen in Fig. 4, good qualitative agreement with experiment below 1.0 eV binding energy is observed in the MO-IPT solution for $U = 5.0\,\text{eV}$. In particular, the energy position of the lower Hubbard band (LHB) at -1.2 eV and the line shape of the total DOS up to 2.5 eV binding energy is in good qualitative agreement with experiment. Moreover, to further demonstrate the important role played by dynamical many-particle interactions in Fig. 4 we also compare our DFT+DMFT results with extant inverse photoelectron spectroscopy (IPS) data for NbO_2 films [52]. Although not perfect, our result for $U = 5.0\,\text{eV}$ qualitatively reproduces the shoulder feature centered around 2.5 eV above E_F in experiment, providing additional support for our orbital-selective electronic structure reconstruction of bct NbO_2.

Taken together, although the structural transition [29] in NbO_2 could be purely of the Peierls type, where dimerization between atoms occurs due to the instability associated with a quasi-one-dimensional chain of Nb atoms, the precise mechanism of this transition is not yet completely understood [24]. However, like for VO_2 [55], it has now been accepted that dimerization of the Nb ions along the c direction in distorted rutile naturally leads to the formation of a band gap in the low-T electronic structure [21,22,25,56] in the framework of a bonding-antibonding splitting [8]. But how this dimer-driven bare insulating state [57] is reshaped by dynamical electron-electron interactions remains a lively open problem of fundamental importance [10,18,39,40]. As already mentioned, similar to that in VO_2 [16], the insulator-metal transition in NbO_2 is predicted to be characterized by a sudden jump [30] in the orbital populations as a consequence, suggesting that anisotropic structural changes will accompany the metal-insulator transition. Thus, we propose that the changes in n_a control anisotropic changes in lattice parameters across the insulator-metal transition: These changes are expressible in terms of n_a as $\gamma_a = \Delta l^a/l^a = (\frac{g}{M v_{sa}^2})\Delta n_a$ [58], where g is the electron-phonon coupling constant, M is the ion mass, and v_{sa} is the velocity of sound along $a\,(\equiv x, y, z)$. Changes in γ_a across the metal-insulator transition thus follow those in n_a. This electron-lattice response, together with the Mott localized features shown in the large-U limit in Figs. 3 and 4, must be taken as an affirmative answer to the chicken-or-the-egg-type debate [6,59] about which comes first, the electronic localization or the lattice distortion in the real crystal. The correct trend vis-á-vis the experiment in Fig. 4 provides further support for a Peierls-to-Mott scenario [60] in NbO_2 and analogs.

III. SUMMARY

In summary, in this paper we analyzed the spectral properties of the dimerized bct phase of NbO_2 in a combined electronic structure and many-body approach. An analytical Green's function formalism was used to calculate the dimerized spectral function for the x^2-y^2 channel of bct NbO_2 along the rutile c axis. The effects of local intra- and interorbital correlations were treated within a multiorbital perturbation approach. We presented results for the local, orbital-resolved density of states and the total spectral function. The latter results were analyzed in comparison with experiments reporting valence [25] and conduction band [52] spectra, showing good qualitative theory-experiment agreement. Our results suggest that bct NbO_2 is a peculiar orbital-selective insulator with Mott (xz, yz) and entangled Mott-Peierls $(x^2$-$y^2)$ localized electrons relevant to future Mott memristors for neuromorphic computing [31] upon external perturbations [61] as well for understanding nonthermal, photoinduced metallicity in which photodoping causes an instantaneous collapse of the band gap without structural modifications [62]. In our DFT+DMFT calculations the insulating regime is best described with a value of $U = 5.0\,\text{eV}$ for the on-site Coulomb interaction. It is important to mention that this result could be achieved only with an appropriate treatment of the dimer-dimer correlations, suggesting that a dimer-embedded DMFT formalism may be appropriate for a correlated description of dimerized multiorbital systems.

ACKNOWLEDGMENTS

I acknowledge CAPES and CNPq as well as S. S. Carara and S. Leoni for helpful comments and discussions.

[1] N. F. Mott, Metal-insulator transition, Rev. Mod. Phys. **40**, 677 (1968).
[2] M. Imada, A. Fujimori, and Y. Tokura, Metal-insulator transitions, Rev. Mod. Phys. **70**, 1039 (1998).
[3] D. Adler, Mechanisms for metal-nonmental transitions in transition-metal oxides and sulfides, Rev. Mod. Phys. **40**, 714 (1968).
[4] Z. Shao, X. Cao, H. Luo, and P. Jin, Recent progress in the phase-transition mechanism and modulation of vanadium dioxide materials, NPG Asia Mater. **10**, 581 (2018).
[5] V. Eyert, The metal-insulator transitions of VO_2: A band theoretical approach, Ann. Phys. (Berlin, Ger.) **514**, 650 (2002).
[6] F. Grandi, A. Amaricci, and M. Fabrizio, Unraveling the Mott-Peierls intrigue in vanadium dioxide, Phys. Rev. Res. **2**, 013298 (2020).
[7] Y.-R. Jo, M.-W. Kim, and B.-J. Kim, Direct correlation of structural and electrical properties of electron-doped individual VO_2 nanowires on devised TEM grids, Nanotechnology **27**, 435704 (2016).
[8] J. B. Goodenough, The two components of the crystallographic transition in VO_2, J. Solid State Chem. **3**, 490 (1971).
[9] A. Zylbersztejn and N. F. Mott, Metal-insulator transition in vanadium dioxide, Phys. Rev. B **11**, 4383 (1975).

[10] S. Biermann, A. Poteryaev, A. I. Lichtenstein, and A. Georges, Dynamical singlets and correlation-assisted Peierls transition in VO_2, Phys. Rev. Lett. **94**, 026404 (2005).

[11] C. Weber, D. D. O'Regan, N. D. M. Hine, M. C. Payne, G. Kotliar, and P. B. Littlewood, Vanadium dioxide: A Peierls-Mott insulator stable against disorder, Phys. Rev. Lett. **108**, 256402 (2012).

[12] M. S. Laad, L. Craco, and E. Müller-Hartmann, Phys. Rev. B **73**, 195120 (2006).

[13] W. H. Brito, M. G. O. Aguiar, K. Haule, and G. Kotliar, Metal-insulator transition in VO_2: A DFT + DMFT perspective, Phys. Rev. Lett. **117**, 056402 (2016).

[14] S. Kim, S. Backes, H. Yoon, W. Kim, C. Sohn, J. Son, S. Biermann, T. W. Noh, and S. Y. Park, Orbital-selective Mott and Peierls transition in H_xVO_2, npj Quantum Mater. **7**, 95 (2022).

[15] R. Wentzcovich, W. Schulz, and P. B. Allen, VO_2: Peierls or Mott-Hubbard? A view from band theory, Phys. Rev. Lett. **72**, 3389 (1994); P. B. Allen, R. Wentzcovich, W. Schulz and P. C. Canfield, Resistivity of the high-temperature metallic phase of VO_2, Phys. Rev. B **48**, 4359 (1993).

[16] M. W. Haverkort, Z. Hu, A. Tanaka, W. Reichelt, S. V. Streltsov, M. A. Korotin, V. I. Anisimov, H. H. Hsieh, H.-J. Lin, C. T. Chen, D. I. Khomskii, and L. H. Tjeng, Orbital-assisted metal-insulator transition in VO_2, Phys. Rev. Lett. **95**, 196404 (2005).

[17] M. S. Laad, L. Craco, and E. Müller-Hartmann, VO_2: A two-fluid incoherent metal? Europhys. Lett. **69**, 984 (2005).

[18] W. H. Brito, M. G. O. Aguiar, K. Haule, and G. Kotliar, Dynamic electronic correlation effects in NbO_2 as compared to VO_2, Phys. Rev. B **96**, 195102 (2017).

[19] L. Craco and S. Leoni, Mott and pseudogap localization in pressurized NbO_2, Phys. Rev. B **102**, 045142 (2020).

[20] G. Kotliar, S. Y. Savrasov, K. Haule, V. S. Oudovenko, O. Parcollet, and C. A. Marianetti, Electronic structure calculations with dynamical mean-field theory, Rev. Mod. Phys. **78**, 865 (2006).

[21] V. Eyert, The metal-insulator transition of NbO_2: An embedded Peierls instability, Europhys. Lett. **58**, 851 (2002).

[22] K. Kulmus, S. Gemming, M. Schreiber, D. Pashov, and S. Acharya, Theoretical evidence for the Peierls transition in NbO_2, Phys. Rev. B **104**, 035128 (2021).

[23] A. O'Hara, T. N. Nunley, A. B. Posadas, S. Zollner, and A. A. Demkov, Electronic and optical properties of NbO_2, J. Appl. Phys. **116**, 213705 (2014).

[24] A. O'Hara and A. A. Demkov, Nature of the metal-insulator transition in NbO_2, Phys. Rev. B **91**, 094305 (2015).

[25] M. J. Wahila *et al.*, Evidence of a second-order Peierls-driven metal-insulator transition in crystalline NbO_2, Phys. Rev. Mater. **3**, 074602 (2019).

[26] W.-C. Lee, M. J. Wahila, S. Mukherjee, C. N. Singh, T. Eustance, A. Regoutz, H. Paik, J. E. Boschker, F. Rodolakis, T.-L. Lee, D. G. Schlom, and L. F. J. Piper, Cooperative effects of strain and electron correlation in epitaxial VO_2 and NbO_2, J. Appl. Phys. **125**, 082539 (2019).

[27] A. K. Cheetham and C. N. R. Rao, A neutron diffraction study of niobium dioxide, Acta Crystallogr., Sect. B **32**, 1579 (1976).

[28] R. F. Janninck and D. H. Whitmore, Electrical conductivity and thermoelectric power of niobium dioxide, J. Phys. Chem. Solids **27**, 1183 (1966); R. Pynn and J. D. Axe, Unusual critical crossover behaviour at a structural phase transformation, J. Phys. C **9**, L199 (1976); K. Seta and K. Naito, Calorimetric study of the phase transition in NbO_2, J. Chem. Thermodyn. **14**, 921 (1982); J. Stoever, J. E. Boschker, S. B. Anooz, M. Schmidbauer, P. Petrik, J. Schwarzkopf, M. Albrecht, and K. Irmscher, Approaching the high intrinsic electrical resistivity of NbO_2 in epitaxially grown films, Appl. Phys. Lett. **116**, 182103 (2020).

[29] A. A. Bolzan, C. Fong, B. J. Kennedy, and C. J. Howard, A powder neutron diffraction study of semiconducting and metallic niobium dioxide, J. Solid State Chem. **113**, 9 (1994).

[30] L. Craco and M. S. Laad, Pseudogap and electron localization in the 4*d* shell of NbO_2 bulk crystal, Phys. Rev. B **108**, 205137 (2023).

[31] S. Kumar, J. P. Strachan, and R. S. Williams, Chaotic dynamics in nanoscale NbO_2 Mott memristors for analogue computing, Nature (London) **548**, 318 (2017).

[32] S. Kim, J. Park, J. Woo, C. Cho, W. Lee, J. Shin, G. Choi, S. Park, D. Lee, B. H. Lee, and H. Hwang, Threshold-switching characteristics of a nanothin-NbO_2-layer-based Pt/NbO_2/Pt stack for use in cross-point-type resistive memories, Microelectron. Eng. **107**, 33 (2013); E. Cha, J. Park, J. Woo, D. Lee, A. Prakash, and H. Hwang, Comprehensive scaling study of NbO_2 insulator-metal-transition selector for cross point array application, Appl. Phys. Lett. **108**, 153502 (2016).

[33] Y. Ran, Y. Pei, Z. Zhou, H. Wang, Y. Sun, Z. Wang, M. Hao, J. Zhao, J. Chen, and X. Yan, A review of Mott insulator in memristors: The materials, characteristics, applications for future computing systems and neuromorphic computing, Nano Res. **16**, 1165 (2023).

[34] M. D. Pickett, G. Medeiros-Ribeiro, and R. S. Williams, A scalable neuristor built with Mott memristors, Nat. Mater. **12**, 114 (2013).

[35] B. Connors, M. Gutnick, and D. Prince, Electrophysiological properties of neocortical neurons in vitro, J. Neurophysiol. **48**, 1302 (1982).

[36] J. K. Clark, Y.-L. Ho, H. Matsui, H. Tabata, and J.-J. Delaunay, Thresholdless behavior and linearity of the optically induced metallization of NbO_2, Phys. Rev. Res. **1**, 033168 (2019).

[37] E. Kamil, R. Schade, T. Pruschke, and P. E. Blöchl, Reduced density-matrix functionals applied to the Hubbard dimer, Phys. Rev. B **93**, 085141 (2016).

[38] R. C. Juliano, A. S. de Arruda, and L. Craco, Coexistence and competition of on-site and intersite Coulomb interactions in Mott-molecular-dimers, Solid State Commun. **227**, 51 (2016).

[39] O. Nájera, M. Civelli, V. Dobrosavljević, and M. J. Rozenberg, Multiple crossovers and coherent states in a Mott-Peierls insulator, Phys. Rev. B **97**, 045108 (2018).

[40] O. Nájera, M. Civelli, V. Dobrosavljević, and M. J. Rozenberg, Resolving the VO_2 controversy: Mott mechanism dominates the insulator-to-metal transition, Phys. Rev. B **95**, 035113 (2017); M. Harland, A. I. Poteryaev, S. V. Streltsov, and A. I. Lichtenstein, Electronic correlations and competing orders in multiorbital dimers: A cluster DMFT study, *ibid.* **99**, 045115 (2019).

[41] A. Georges, G. Kotliar, W. Krauth, and M. J. Rozenberg, Dynamical mean-field theory of strongly correlated fermion systems and the limit of infinite dimensions, Rev. Mod. Phys. **68**, 13 (1996).

[42] L. Fratino, S. Bag, A. Camjayi, M. Civelli, and M. Rozenberg,

Doping-driven resistive collapse of the Mott insulator in a minimal model for VO_2, Phys. Rev. B **105**, 125140 (2022).

[43] L. Craco, Quantum orbital entanglement: A view from the extended periodic Anderson model, Phys. Rev. B **77**, 125122 (2008).

[44] A. Koga, N. Kawakami, T. M. Rice, and M. Sigrist, Spin, charge, and orbital fluctuations in a multiorbital Mott insulator, Phys. Rev. B **72**, 045128 (2005).

[45] L. Craco, M. S. Laad, S. Leoni, and E. Müller-Hartmann, Insulator-metal transition in the doped $3d^1$ transition metal oxide, Phys. Rev. B **70**, 195116 (2004).

[46] The on-site orbital energies of for the *xz* and *yz* orbitals are read off from DFT spectral functions.

[47] L. Craco and S. Leoni, Theory of two-fluid metallicity in superconducting FeSe at high pressure, Phys. Rev. B **100**, 121101(R) (2019).

[48] We use the same J_H value as in Refs. [18,19,26].

[49] A. Liebsch, Doping-driven Mott transition in $La_{1-x}Sr_xTiO_3$ via simultaneous electron and hole doping of t_{2g} subbands as predicted by LDA+DMFT calculations, Phys. Rev. B **77**, 115115 (2008); L. Craco and S. Leoni, Orbital-selective mixed-valent Mott/metal phase coexistence in $NdNiO_2$ films, Phys. Rev. Mater. **7**, 044802 (2023).

[50] M. S. Laad, L. Craco, and E. Müller-Hartmann, Orbital switching and the first-order insulator-metal transition in paramagnetic V_2O_3, Phys. Rev. Lett. **91**, 156402 (2003); L. Craco, M. S. Laad, S. Leoni, and H. Rosner, Theory of the orbital-selective Mott transition in ferromagnetic $YTiO_3$ under high pressure, Phys. Rev. B **77**, 075108 (2008).

[51] Using the converged DOS for each orbital, at fixed $\Phi = -0.6\,\text{eV}$ and $U = 3.5\,\text{eV}$, the obtained DFT + DMFT orbital occupancies are $(n_{x^2-y^2}, n_{xz}, n_{yz}, n_{xy}) = (0.62, 0.22, 0.16)$. These selective occupations change to $(n_{x^2-y^2}, n_{xz}, n_{yz}, n_{xy}) = (0.46, 0.46, 0.08)$ at $U = 4.5\,\text{eV}$.

[52] A. B. Posadas, A. O'Hara, S. Rangan, R. A. Bartynski, and A. A. Demkov, Band gap of epitaxial in-plane-dimerized single-phase NbO_2 films, Appl. Phys. Lett. **104**, 092901 (2014).

[53] Y. Liu, H. Zhang, and X. Cheng, Sequential insulating-metal-insulating phase transition of NbO_2 by doping photoexcited carrier, Comput. Mater. Sci. **173**, 109434 (2020).

[54] The DFT plus continuous time quantum Monte Carlo (CT-QMC) work by Brito *et al.* [18] derives the many-body total DOS at $T = 1000$ K considering $U = 6.0\,\text{eV}$.

[55] W. R. Mondal, E. Evlyukhin, S. A. Howard, G. J. Paez, H. Paik, D. G. Schlom, L. F. J. Piper, and W.-C. Lee, Role of V-V dimers on structural, electronic, magnetic, and vibrational properties of VO_2 by first-principles simulations and Raman spectroscopic analysis, Phys. Rev. B **103**, 214107 (2021).

[56] G. J. P. Fajardo, S. A. Howard, E. Evlyukhin, M. J. Wahila, W. R. Mondal, M. Zuba, J. E. Boschker, H. Paik, D. G. Schlom, J. T. Sadowski, S. A. Tenney, B. Reinhart, W.-C. Lee, and L. F. J. Piper, Structural phase transitions of NbO_2: Bulk versus surface, Chem. Mater. **33**, 1416 (2021).

[57] D. Kartoon, U. Argaman, and G. Makov, Driving forces behind the distortion of one-dimensional monatomic chains: Peierls theorem revisited, Phys. Rev. B **98**, 165429 (2018).

[58] L. Craco, M. S. Laad, and S. Leoni, Microscopic description of insulator-metal transition in high-pressure oxygen, Sci. Rep. **7**, 2632 (2017).

[59] D. Shiga, B. E. Yang, N. Hasegawa, T. Kanda, R. Tokunaga, K. Yoshimatsu, R. Yukawa, M. Kitamura, K. Horiba, and H. Kumigashira, Thickness dependence of electronic structures in VO_2 ultrathin films: Suppression of the cooperative Mott-Peierls transition, Phys. Rev. B **102**, 115114 (2020); Y. Zhang, L.-F. Lin, A. Moreo, and E. Dagotto, Orbital-selective Peierls phase in the metallic dimerized chain $MoOCl_2$, *ibid.* **104**, L060102 (2021).

[60] H. Fehske, A. P. Kampf, M. Sekania, and G. Wellein, Nature of the Peierls- to Mott-insulator transition in 1D, Eur. Phys. J. B **31**, 11 (2003).

[61] J. Park, E. Cha, I. Karpov, and H. Hwang, Dynamics of electroforming and electrically driven insulator-metal transition in NbO_x selector, Appl. Phys. Lett. **108**, 232101 (2016); S. Kumar, Z. Wang, N. Davila, N. Kumari, K. J. Norris, X. Huang, J. P. Strachan, D. Vine, A. L. D. Kilcoyne, Y. Nishi, and R. S. Williams, Physical origins of current and temperature controlled negative differential resistances in NbO_2, Nat. Commun. **8**, 658 (2017); D. S. Jeon, T. D. Dongale, and T. G. Kim, Low power Ti-doped NbO_2-based selector device with high selectivity and low off current, J. Alloys Compd. **884**, 161041 (2021); A. Chen, Y. Fu, G. Ma, G. Yang, N. Liu, X. Zhao, Z. Zhang, L. Tao, H. Wan, Y. Rao, J. Duan, L. Shen, J. Zhang, P. Sun, D. Yang, T.-C. Chang, and H. Wang, The Co-improvement of selectivity and uniformity on NbO_x-based selector by Al-doping, IEEE Electron Device Lett. **43**, 870 (2022).

[62] R. Rana, J. M. Klopf, J. Grenzer, H. Schneider, M. Helm, and A. Pashkin, Nonthermal nature of photoinduced insulator-to-metal transition in NbO_2, Phys. Rev. B **99**, 041102(R) (2019).